


## Cosmic QCD transition: From quark to strangeon nugget and nucleon?

Xuhao Wu 

*Key Laboratory for Microstructural Material Physics of Hebei Province,  
School of Science, Yanshan University,  
Qinhuangdao 066004, China*

*School of Physics, Peking University,  
Beijing 100871, China*

*Kavli Institute for Astronomy and Astrophysics,  
Peking University, Beijing 100871, China  
wuhaobird@gmail.com*


Weibo He\* and Yudong Luo 

*School of Physics, Peking University,  
Beijing 100871, China*

*Kavli Institute for Astronomy and Astrophysics,  
Peking University, Beijing 100871, China*

\*webb\_he@stu.pku.edu.cn

†yudong.luo@pku.edu.cn

Guo-Yun Shao 

*School of Science, Xi'an Jiaotong University,  
Xi'an 710049, China*

*MOE Key Laboratory for Nonequilibrium Synthesis  
and Modulation of Condensed Matter,  
Xi'an Jiaotong University, Xi'an 710049, China  
gyshao@mail.xjtu.edu.cn*

Ren-Xin Xu 

*School of Physics, Peking University,  
Beijing 100871, China*

*Kavli Institute for Astronomy and Astrophysics,  
Peking University, Beijing 100871, China  
r.x.xu@pku.edu.cn*

Received 25 January 2024

Revised 11 March 2024

Accepted 15 April 2024

Published 25 June 2024

We investigate a crossover quantum chromodynamical (QCD) phase transition that occurred in the early Universe and explore a potential formation scenario for stable strangeon nuggets during this process. To analyze the thermodynamics of the QCD phase involving  $u$ ,  $d$ ,  $s$  quarks, we employ the Polyakov–Nambu–Jona-Lasinio model, while the relativistic mean-field model is used to describe the hadronic matter. We consider the participation of strangeons (strange quark clusters with net strangeness) in the quark-hadron phase transition process. During this process, strangeon nuggets are formed, and larger nuggets could survive after the phase transition. The crossover phase transition from quarks to hadrons occur at a cosmic temperature of approximately  $T \sim 170$  MeV, and these two phases (quark phase and strangeon nugget-hadronic phase) are connected in a three-window model. We introduce a distribution function of the nugget baryon number,  $A$ , to describe the nugget’s number density (equivalent to the mass spectrum). All strangeon nuggets with  $A > A_c$  are considered to be stable, where the critical number,  $A_c$ , is determined by both weak and strong interactions. To calculate the thermodynamics of stable strangeon nuggets, a nonrelativistic equation of state was applied, resulting in negligible thermodynamic contributions (pressure, entropy, etc.) compared to the hadronic part. Our study shows that the mass fraction of the strangeon nuggets that survived from the early Universe is comparable to dark matter, suggesting a possible explanation for cold dark matter without introducing any exotic particles beyond the Standard Model.

*Keywords:* Cosmic QCD; strangeon nuggets; dark matter.

PACS Number(s): 95.35.+d, 98.80.Bp

## 1. Introduction

Cosmic phase transitions<sup>1–4</sup> are natural consequences of hot big bang cosmology, playing a crucial role in understanding various cosmological phenomena such as the primordial magnetic field,<sup>5</sup> baryonic asymmetry<sup>6,7</sup> and even the gravitational wave background.<sup>8,9</sup> In the early Universe, at least two types of transitions occurred: the quantum chromodynamical (QCD) phase transition<sup>10</sup> and the electroweak (EW) transition.<sup>11</sup> The EW transition occurs when the cosmic temperature drops below  $T \sim 10^2$  MeV, breaking the EW symmetry and allowing particles within the Standard Model to acquire gauge-invariant masses.<sup>13,12</sup> On the other hand, the exact dynamics of the QCD phase transition remains unclear, as perturbation theory breaks down during this process. If the QCD transition is of first order, stable quark nuggets (strangelet) with a large baryon number may survive.<sup>14</sup> However, the transition is likely to be a rapid and smooth crossover,<sup>15–17</sup> according to lattice QCD simulations and various effective QCD models. A question arises: Could the real nature of dark matter be strangelet that survived from the early Universe? This question has been extensively studied since Witten’s work in 1984.<sup>14</sup> Strangelet, a candidate for dark matter, has even been proposed as a potential explanation for the puzzling presence of supermassive black holes at high redshifts,<sup>18</sup> invoking their rapid formation into stellar-mass black holes.<sup>19</sup> However, in our study, we consider strangeon nuggets instead of quark nuggets (strangelets) as dark matter candidate, as they are formed through strong interactions at the hadron level. Unlike strangelets, which consist of quarks bound by strong interactions at the quark level, strangeon nuggets possess stronger interactions and potentially greater stability. Furthermore, it is important to note that the strangeon nuggets we mentioned are

the outcome of a crossover QCD phase transition, in contrast to strangelets which arise from a first-order QCD phase transition. Therefore, the focus of this work is to investigate the QCD crossover transition and the potential role of the production of strangeon nuggets.

After the EW phase transition, the Universe becomes filled with a dense and hot quark–gluon plasma (QGP) consisting of six flavors of quarks. This state persists until the temperature drop to a few giga-electronvolts. At this point, the heavy flavors of quarks, namely charm ( $c$ ), top ( $t$ ) and bottom ( $b$ ) quarks with masses greater than 1 GeV, begin to decay into lighter quarks: up ( $u$ ), down ( $d$ ) and strange ( $s$ ) quarks, whose masses are approximately less than 0.1 GeV. This process occurs under the chemical equilibrium. Subsequently, the Universe enters the QCD phase transition. During this epoch, the initial phase of strongly interacting quark matter at temperatures above or equal to 100 MeV gradually transforms into hadronic matter, predominantly composed of nucleons, as the temperature decreased to around 10 MeV. This phase transition provides the initial conditions for the subsequent process known as big bang nucleosynthesis (BBN), which is responsible for the production of light elements in the early Universe. The cosmic timeline of this epoch is illustrated in Fig. 1.<sup>20,21</sup>

In a model of first-order cosmological QCD phase transition, low-temperature bubbles emerge once the cosmic temperature falls below the critical temperature  $T_c \sim (100 - 200)$  MeV.<sup>14</sup> These bubbles release heat to the surrounding high-temperature phase, gradually expanding and colliding. As the Universe expands and the temperature continues to decrease, these dense and high-temperature bubbles eventually become isolated. They lose energy through surface evaporation and neutrino emission, with the latter carrying only the leptons away while leaving the baryons trapped inside the bubbles. Consequently, the baryon excess within the bubbles eventually reaches a stable state, i.e. the strangelet.

However, whether the QCD phase diagram has first-order phase transitions is still a subject of ongoing debate. In particular, when considering the chiral phase transition, it is necessary for the evolution line to terminate at the critical point. At a cosmic temperature above 100 MeV, three flavors of quarks ( $u$ ,  $d$ ,  $s$ ) coexist in an equilibrium state. Besides the first-order phase transition, it is also reasonable to consider a smooth crossover phase transition starting from the QGP phase with free quarks to hadrons. This notion finds support in lattice QCD simulations and

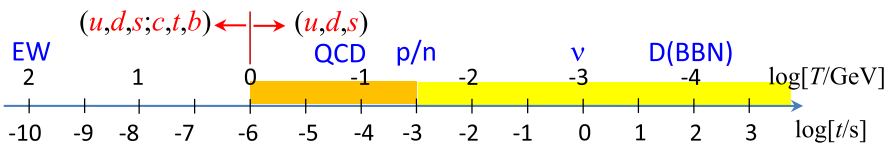


Fig. 1. Cosmic evolution from the EW epoch to the BBN. Free nucleons (protons and neutrons,  $p/n$ ) appear after QCD phase transition at  $T \sim 100$  MeV, setting the initial condition of BBN. Neutrinos ( $\nu$ ) are decoupled at  $T \sim 1$  MeV, while the deuterium (D) forms at  $T \sim 0.1$  MeV.

numerous effective QCD models, which suggest that the transition is more likely to be a simple crossover rather than a first-order transition.<sup>15,16,22</sup> During the crossover QCD phase transition, quarks can undergo collisions, leading to the formation of nucleon-like clusters containing strangeness. These clusters, referred to as “strangeons” (a term coined by combining “strange” and “nucleon”<sup>23</sup>), may nucleate and subsequently merge and collide, eventually giving rise to nuggets composed of strangeons, i.e. the strangeon nuggets. Hot strangeon nuggets, at cosmic temperatures above approximately 100 MeV,<sup>24,25</sup> may have the ability to emit particles such as strangeons,  $\Lambda$  and nucleon. Eventually, they decay into neutrons and protons.<sup>26</sup> As the temperature decreases, the process of evaporation becomes suppressed, allowing the remaining strangeon nuggets to reach a state of thermodynamic stability. These stable nuggets can persist if they possess a sufficient number of baryons. It is important to note that there is difference between strangeon nuggets and strangelets as proposed in Ref. 14. Strangelets consist of  $u$ ,  $d$  and  $s$  quarks and can only be stable if they contain an initial baryon number over the order of  $\sim 10^{44}$ .<sup>24,25,27,28</sup> Similar to atomic nuclei, which remain stable due to the interactions (both strong and weak) between protons and neutrons, strangeon nuggets are composed of strangeons as their fundamental units. Consequently, heavy strangeon nuggets can also exhibit stability as a result of these weak and strong interactions.<sup>29</sup>

Many previous studies have investigated the strangeon matter from the astrophysical perspective,<sup>30</sup> aiming to solve the problem raised by Lev Landau more than 90 years ago.<sup>31</sup> It is believed that strangeon stars, which are stellar-sized strangeon nuggets, can provide an explanation for certain pulsar observations. While neutron stars have traditionally been considered, previous works<sup>32,33</sup> indicated that bare strangeon stars could account for the sub-pulse drift signal, and Refs. 34 and 35 showed further the potential of strangeon stars to explain the observed relative glitch amplitude. Furthermore, several theoretical research studies<sup>36–38</sup> studied the pulsar glitches mechanism in the framework of the strangeon stars. The global parameters of rotating strangeon stars and the oscillation modes of nonrotating strangeon stars have also been investigated in full general relativity by Refs. 39 and 40, respectively. In relation to strange quark matter in the early Universe, a recent study discusses the possibility to destroy primordial  ${}^7\text{Li}$  abundance via a 2 MeV photo emission line from color superconducting quark nuggets.<sup>41</sup> Our previous work<sup>19</sup> investigated the possibility that strangeon nuggets formed during the QCD phase transition could collapse to a stellar-mass black hole, then it kept growing by the gas accretion and became the supermassive black hole at redshift  $z > 6$ .

This work explores the behavior of strangeon nuggets in the context of the crossover QCD phase transition in the early Universe. The  $s$ -quark itself is not stable and undergoes decay via  $s \rightarrow e^- + u + \bar{\nu}_e$  with a lifetime of approximately  $\sim 10^{-9}$  s. However, there exists a threshold baryon number  $A_c$  which determines whether a strangeon nugget will undergo evaporation due to weak interactions. If a small

strangeon nugget has  $A < A_c$ , it will be completely destroyed by weak interaction-induced evaporation. Conversely, a large strangeon nugget will remain stable, as the decay of a significant number of  $s$ -quarks into  $u/d$ -quarks simultaneously through weak interactions is highly unlikely. During a crossover phase transition, strangeon nuggets are formed through collision and nucleation. As a result, their baryon number may not be as large as those produced during a first-order phase transition (where  $A_c \sim 10^{44}$ ). Additionally, the distribution of these nuggets may not be uniform. Relic nuggets with small baryon numbers could potentially interact with nuclei during the epoch of primordial nucleosynthesis. Further investigations on such interactions could provide more stringent constraints. On the other hand, strangeon nuggets with large baryon numbers would interact negligibly with normal baryonic matter through strong, weak or electromagnetic interactions. This makes the strangeon nuggets potential candidates for cold dark matter (CDM).

In fact, there are several potential candidates of the CDM: axion, weakly interacting massive particles (WIMPs), primordial black holes, etc.<sup>21</sup> Axions and WIMPs are hypothetical elementary particles that are not part of the Standard Model. To produce primordial black holes which appear before the QCD transition, a significant density fluctuation is required in the early Universe, as discussed in Refs. 21, 42 and 43. Many proposed extensions to the Standard Model have been ruled out, leading to a narrowing of the allowed parameter space.<sup>44,45</sup> One motivation for this study is that stable strangeon nuggets provide a potential candidate for dark matter within the realm of “old” physics, without invoking any exotic particles. The connection between strangeness and dark matter has a long history, as discussed in Refs. 14 and 45–48, due to the low charge-to-mass ratio if the symmetry of light-quark flavors ( $u$ ,  $d$  and  $s$ ) is restored.

This study describes quark matter using the Polyakov–Nambu–Jona-Lasinio (PNJL) model, which accounts for asymptotic freedom, chiral symmetry restoration at high density, and quark confinement as signified by the Polyakov loop. This model extends the Nambu–Jona-Lasinio (NJL) model, providing an effective theoretical framework for low-energy QCD that incorporates all QCD symmetries in its Lagrangian. The interaction between fermions in the PNJL model occurs through the coupling of local fermions, while gluon degrees of freedom are constrained in quark-like point interactions. We utilize the relativistic mean-field (RMF) model to describe hadronic matter, which is an effective field theory approach based on meson exchange theory. In the RMF model, meson masses and various coupling constants in the Lagrangian are free parameters that can be adjusted to fit experimental data and nuclear matter saturation properties.

This paper is organized as follows. In Sec. 2, we provide a brief introduction to the PNJL model for quark matter in the QGP phase and the RMF model for the hadron phase. In Sec. 3, we examine the formation of strangeon nuggets and the crossover QCD phase transition. Section 4 presents the numerical results and discussions of the QCD phase transition. Section 5 provides a summary of our findings.

## 2. Equations of State of Quark Phase and Hadronic Phase

During the QCD phase transition, the statistical equilibrium and the charge neutrality are satisfied. Figure 2 presents the conjectured QCD phase diagram in the  $T$ - $\mu_B$  plane (for quantitative discussions on the QCD phase diagram, refer to Refs. 49–51). The first-order nuclear liquid–gas phase transition (solid black line in Fig. 2) occurs at low temperatures, where  $\mu_B$  is approximately equal to the nucleon mass. The hadron–quark phase transition is a crossover (blue dashed line) at high temperatures and a first-order transition (solid blue line) at low temperatures. These two lines are connected by the critical end point (red dot). Although the exact curve that distinguishes the QGP phase and hadron gas phase has not yet been determined, current experiments and theories provide an overview of the diagram. At low temperatures and extremely large  $\mu_B$ , various forms of quark Cooper pairing, such as the color superconducting phase, may appear. We consider the trajectory of the Universe in the QCD phase diagram to follow a crossover phase transition, nearly approaching the vertical axis with almost zero chemical potential. The temperature  $T$  begins from  $T \sim 200$  MeV to approach the nuclear matter region at low temperatures ( $T \sim 1$  MeV).

In general, the equation of state (EOS) of the QGP phase and the hadron–strangeon (HS) nuggets phase under finite temperature depends on the number density and one of these thermodynamical quantities: temperature, entropy density or lepton fraction  $Y_l$ . In this study, the thermodynamical quantities are considered as functions of temperature  $T$  and entropy per baryon  $s/n_b$ . It is assumed that the Universe maintains isentropic during its expansion. In the case of relativistic particles, the entropy of the Universe is primarily contributed by the relativistic gas,<sup>20,52,53</sup> and the entropy density  $s$  is proportional to the number

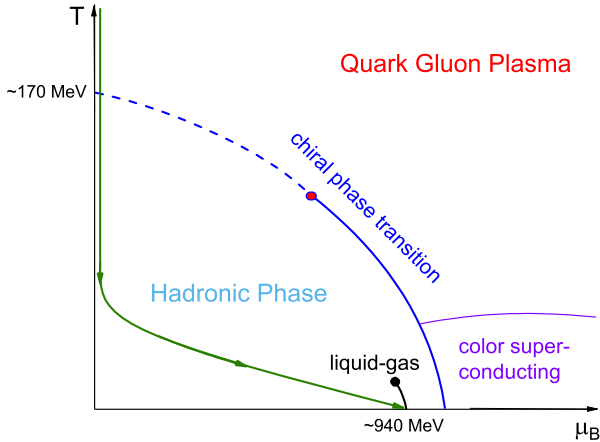


Fig. 2. (Color online) Sketch of the QCD phase diagram in terms of temperature  $T$  and baryon chemical potential  $\mu_B$ . The green curve with arrows illustrates the thermal trajectory of the Universe during the QCD epoch.

of particles,

$$s \equiv \frac{S}{V} = \frac{\varepsilon + p}{T} = \frac{2\pi^2}{45} g_{*s} T^3, \quad (1)$$

where  $g_{*s}$  is the sum of the degrees of freedom for all relativistic particles.  $\varepsilon$  and  $p$  are the energy density and pressure, respectively. Since most of the time, these particles share the same temperature, the entropy density  $s$  is proportional to the photon number density,  $s = 1.80g_{*s}n_\gamma$ . The entropy per baryon  $s/n_b$  remains constant with respect to the co-moving frame of reference since  $n_b \propto T^3$ . The value of  $s/n_b$  can be obtained from the baryon-to-photon ratio  $\eta$  using the relation  $\eta = 1.8g_{*s}(n_b/s)$ . Observations of the cosmic microwave background power spectrum currently constrain  $\eta$  to be  $(6.16 \pm 0.02) \times 10^{-10}$ , which corresponds to a baryon density of  $\Omega_b h^2 = 0.0224 \pm 0.0001$  within the standard  $\Lambda$ CDM model.<sup>54</sup> In this study, we adopt the value of  $s/n_b$  based on this  $\eta$  value. Furthermore, we also consider an extreme alternative scenario with  $s/n_b = 100$  for compression.

## 2.1. Quark phase

To describe the  $u - d - s$  quark matter, we employ the three-flavor PNJL model, which is constructed by SU(3) NJL model coupled to a temporal background gauge field representing Polyakov loop dynamics. The effective Lagrangian is written as (hereafter, we use the natural unit  $c = \hbar = k_B = 1$ )

$$\begin{aligned} \mathcal{L}_{\text{PNJL}} = & \bar{q}(i\gamma_\mu D^\mu - m^0)q + G \sum_{a=0}^8 [(\bar{q}\lambda_a q)^2 + (\bar{q}i\gamma_5\lambda_a q)^2] \\ & - K \{ \det[\bar{q}(1 + \gamma_5)q] + \det[\bar{q}(1 - \gamma_5)q] \} - \mathcal{U}(\bar{\Phi}, \Phi, T), \end{aligned} \quad (2)$$

where  $q(\bar{q})$  denotes a quark (antiquark) field with three flavors ( $N_f = 3$ ) and three colors ( $N_c = 3$ ).  $m^0 = \text{diag}(m_u^0, m_d^0, m_s^0)$  is the current quark mass matrix, and we assume isospin symmetry  $m_u^0 = m_d^0 \equiv m_q^0$ .  $\lambda_a (a = 1, \dots, 8)$  and  $\gamma_\mu (\mu = 0, 1, 2, 3)$  represent the Gell-Mann matrices and the Dirac matrices, while  $\lambda_0 = \sqrt{2/3}I$  ( $I$  is the unit matrix),  $\gamma_5 = i\gamma_0\gamma_1\gamma_2\gamma_3$ . We use the parameters in Ref. 55,  $m_q^0 = 5.5 \text{ MeV}$ ,  $m_s^0 = 140.7 \text{ MeV}$ ,  $\Lambda = 603.2 \text{ MeV}$ ,  $G\Lambda^2 = 1.835$ ,  $K\Lambda^5 = 12.36$ . The quantity  $\mathcal{U}(\bar{\Phi}, \Phi, T)$  is the effective potential in terms of  $\bar{\Phi}$  and  $\Phi$ ,

$$\Phi = (\text{Tr}_c L)/N_c, \quad (3)$$

$$\bar{\Phi} = (\text{Tr}_c L^+)/N_c, \quad (4)$$

which are the traced Polyakov loop and its conjugate. A logarithmic formed Polyakov loop potential  $\mathcal{U}(\Phi, \bar{\Phi}, T)$  is applied<sup>56</sup>

$$\frac{\mathcal{U}(\Phi, \bar{\Phi}, T)}{T^4} = -\frac{b_2(T)}{2} \bar{\Phi}\Phi - b_4(T) \ln[1 - 6\bar{\Phi}\Phi + 4(\bar{\Phi}^3 + \Phi^3) - 3(\bar{\Phi}\Phi)^2], \quad (5)$$

Table 1. Dimensionless parameters of the potentials and  $T_0$  given in Eqs. (5) and (6).<sup>56</sup>

$a_0$	$a_1$	$a_2$	$a_3$	$b_3$	$b_4$	$T_0$
6.75	-1.95	2.625	-7.44	0.75	7.5	270 MeV

with

$$b_2(T) = a_0 + a_1 \left( \frac{T_0}{T} \right) + a_2 \left( \frac{T_0}{T} \right)^2, \quad (6)$$

$$b_4(T) = b_4 \left( \frac{T_0}{T} \right)^3,$$

where  $T_0$  represents a characteristic temperature at which  $\Phi$  undergoes a transition from a vanishing value to a finite value. The parameters are provided in Table 1.

$\Phi$  and  $\bar{\Phi}$  are determined by

$$\frac{\partial \Omega}{\partial \phi_i} = 0, \quad (7)$$

$$\frac{\partial \Omega}{\partial \Phi} = 0, \quad \frac{\partial \Omega}{\partial \bar{\Phi}} = 0, \quad (8)$$

$\Omega$  is the grand canonical potential

$$\Omega = U(\bar{\Phi}, \Phi, T) + 2G(\phi_u^2 + \phi_d^2 + \phi_s^2) - 4K\phi_u\phi_d\phi_s - 2N_c \int_{\Lambda} \frac{d^3k}{(2\pi)^3} (E_u + E_d + E_s)$$

$$- 2 \sum_{i=u,d,s} \int \frac{d^3k}{(2\pi)^3} \frac{k^2}{E_i^2} [F^+(E_i - \mu_i, T, \Phi, \bar{\Phi}) + F^-(E_i + \mu_i, T, \Phi, \bar{\Phi})], \quad (9)$$

with

$$F^+(x, T, \Phi, \bar{\Phi}) = \frac{\Phi e^{-x/T} + 2\bar{\Phi} e^{-2x/T} + e^{-3x/T}}{1 + 3\bar{\Phi} e^{-x/T} + 3\bar{\Phi} e^{-2x/T} + e^{-3x/T}}, \quad (10)$$

$$F^-(x, T, \Phi, \bar{\Phi}) = \frac{\bar{\Phi} e^{-x/T} + 2\Phi e^{-2x/T} + e^{-3x/T}}{1 + 3\bar{\Phi} e^{-x/T} + 3\bar{\Phi} e^{-2x/T} + e^{-3x/T}}, \quad (11)$$

being the generalized Fermi–Dirac distribution, where  $E_i = \sqrt{k^2 + m_i^2}$ . The constituent quark mass obeys the gap equation

$$m_i = m_i^0 - 4G\phi_i + 2K\phi_j\phi_k, \quad (12)$$

where  $\phi_i$  is the quark condensate. The quark number density can be expressed as

$$n = \rho_v = 2N_c N_f \int_0^\infty \frac{k^2 dk}{2\pi^2} (F^+ - F^-). \quad (13)$$

Through thermodynamic relations, one can derive expressions for various thermodynamic quantities. The expressions of the pressure  $P$ , the energy density  $\varepsilon$ , the



entropy density  $s$  and the free energy density  $f$  are provided as

$$P_{\text{PNJL}} = -\mathcal{U}(\bar{\Phi}, \Phi, T) - 2G(\phi_u^2 + \phi_d^2 - \phi_s^2) + 4K\phi_u\phi_d\phi_s \\ + 2N_c N_f \frac{1}{3} \int_0^\infty \frac{k^2 dk}{2\pi^2} \frac{k^2}{E_i} (F^+ + F^-) + 2N_c N_f \int_0^\Lambda \frac{k^2 dk}{2\pi^2} E_i + \varepsilon_{\text{vac}}, \quad (14)$$

$$\varepsilon_{\text{PNJL}} = \mathcal{U}(\bar{\Phi}, \Phi, T) - T \frac{\partial \mathcal{U}}{\partial T} + 2G(\phi_u^2 + \phi_d^2 - \phi_s^2) - 4K\phi_u\phi_d\phi_s \\ + 2N_c N_f \int_0^\infty \frac{k^2 dk}{2\pi^2} E_i (F^+ + F^-) - 2N_c N_f \int_0^\Lambda \frac{k^2 dk}{2\pi^2} E_i - \varepsilon_{\text{vac}}, \quad (15)$$

$$s_{\text{PNJL}} = -\frac{\partial \mathcal{U}}{\partial T} + 2N_c N_f \frac{1}{3} \frac{1}{T} \int_0^\infty \frac{k^2 dk}{2\pi^2} \frac{k^2}{E_i} (F^+ + F^-) \\ + 2N_c N_f \frac{1}{T} \int_0^\infty \frac{k^2 dk}{2\pi^2} E_i (F^+ + F^-) - 2N_c N_f \frac{\mu}{T} \int_0^\infty \frac{k^2 dk}{2\pi^2} (F^+ - F^-), \quad (16)$$

$$f_{\text{PNJL}} = \varepsilon_{\text{PNJL}} - T s_{\text{PNJL}}. \quad (17)$$

Inside the homogeneous matter, leptons (and anti-leptons) occupy single-particle states with the Fermi–Dirac distribution. The particle and antiparticle occupation probability is given by

$$f_i^k = [1 + e^{(E_i^k - \mu_i)/T}]^{-1}, \quad (18)$$

$$f_{\bar{i}}^k = [1 + e^{(E_i^k + \mu_i)/T}]^{-1}, \quad (19)$$

respectively. The leptons are treated as free Fermi gas, and their thermodynamic quantities can be described by the following expressions:

$$P_l = \frac{1}{3} \sum_{l=e,\mu} \frac{1}{\pi^2} \int \frac{k^4}{(k^2 + m_l^2)^{1/2}} (f_l^k + f_{\bar{l}}^k) dk, \quad (20)$$

$$\varepsilon_l = \sum_{l=e,\mu} \frac{1}{\pi^2} \int (k^2 + m_l^2)^{1/2} k^2 (f_l^k + f_{\bar{l}}^k) dk, \quad (21)$$

$$s_l = \sum_{l=e,\mu} \frac{1}{\pi^2} \int dk [-f_l^k \ln f_l^k - (1 - f_l^k) \ln(1 - f_l^k) \\ - f_{\bar{l}}^k \ln f_{\bar{l}}^k - (1 - f_{\bar{l}}^k) \ln(1 - f_{\bar{l}}^k)], \quad (22)$$

$$f_l = \varepsilon_l - T s_l. \quad (23)$$

By incorporating the contributions from both leptons and quarks, we obtain the expressions of quark phase,

$$P_Q = P_{\text{PNJL}} + P_l, \quad (24)$$

$$\varepsilon_Q = \varepsilon_{\text{PNJL}} + \varepsilon_l, \quad (25)$$

$$s_Q = s_{\text{PNJL}} + s_l, \quad (26)$$

$$f_Q = \varepsilon_Q - T s_Q. \quad (27)$$

## 2.2. Hadronic phase

To describe the hadronic matter, we utilize the RMF theory, which could successfully predict experimental data of finite nuclei and saturation properties at low densities. The Lagrangian reads

$$\begin{aligned} \mathcal{L}_{\text{RMF}} = & \sum_{i=p,n} \bar{\psi}_i \left\{ i\gamma_\mu \partial^\mu - (M + g_\sigma \sigma) - \gamma_\mu \left[ g_\omega \omega^\mu + \frac{g_\rho}{2} \tau_a \rho^{a\mu} \right] \right\} \psi_i \\ & + \frac{1}{2} \partial_\mu \sigma \partial^\mu \sigma - \frac{1}{2} m_\sigma^2 \sigma^2 - \frac{1}{3} g_2 \sigma^3 - \frac{1}{4} g_3 \sigma^4 - \frac{1}{4} W_{\mu\nu} W^{\mu\nu} + \frac{1}{2} m_\omega^2 \omega_\mu \omega^\mu \\ & - \frac{1}{4} R_{\mu\nu}^a R^{a\mu\nu} + \frac{1}{2} m_\rho^2 \rho_\mu^a \rho^{a\mu} + \sum_{l=e,\mu} \bar{\psi}_l (i\gamma_\mu \partial^\mu - m_l) \psi_l, \end{aligned} \quad (28)$$

where  $W^{\mu\nu}$  and  $R^{\alpha\mu\nu}$  are the antisymmetric field tensors,

$$\begin{aligned} W^{\mu\nu} &= \partial^\mu \omega^\nu - \partial^\nu \omega^\mu, \\ R^{\alpha\mu\nu} &= \partial^\mu \omega^{\alpha\nu} - \partial^\nu \omega^{\alpha\mu} + g_\rho \varepsilon^{\alpha\beta\gamma} \rho^{\beta\mu} \rho^{\gamma\nu}. \end{aligned}$$

In the RMF model, the interactions among hadrons are described by the exchange of mesons. Specifically, the  $\sigma$  meson accounts for the mid-range attraction, while the  $\omega$  meson represents the short-range repulsion, and the  $\rho$  meson takes into account the isospin difference between neutrons and protons. The masses of these mesons, along with the corresponding coupling constants, are provided in Table 2. Hadronic matter satisfies the statistical equilibrium and charge neutrality condition, i.e.

$$\mu_n = \mu_p + \mu_e, \quad (29)$$

$$\mu_\mu = \mu_e, \quad (30)$$

$$n_p = n_e + n_\mu. \quad (31)$$

The vector density and the scalar density are given by

$$n_i = \rho_v = \langle \bar{\psi}_b \gamma_0 \psi_b \rangle = \frac{1}{\pi^2} \int k^2 (f_i^k - f_{\bar{i}}^k) dk, \quad (32)$$

$$\rho_s = \langle \bar{\psi}_b \psi_b \rangle = \frac{1}{\pi^2} \int \frac{m_N^*}{E^*} k^2 (f_i^k + f_{\bar{i}}^k) dk, \quad (33)$$

Table 2. Parameters in the GM1 model.<sup>57</sup> The masses are given in MeV.

Model	$M$	$m_\sigma$	$m_\omega$	$m_\rho$	$g_\sigma$	$g_\omega$	$g_\rho$	$g_2$ (fm <sup>-1</sup> )	$g_3$
GM1	938.000	550.000	783.000	770.000	9.5705	10.6096	8.1954	-12.2799	-8.9767

respectively. The energy density  $\varepsilon$ , pressure  $P$ , entropy density  $s$  and free energy density  $f$  of the hadron phase can be expressed as follows:

$$\begin{aligned} \varepsilon_{\text{H}} = & \frac{1}{2} m_{\sigma}^2 \sigma^2 + \frac{1}{3} g_2 \sigma^3 + \frac{1}{4} g_3 \sigma^4 + \frac{1}{2} m_{\omega}^2 \omega^2 + \frac{1}{2} m_{\rho}^2 \rho^2 \\ & + \sum_{i=n,p} \frac{1}{\pi^2} \int (k^2 + m_N^{*2})^{1/2} k^2 (f_i^k + \bar{f}_i^k) dk + \varepsilon_l, \end{aligned} \quad (34)$$

$$\begin{aligned} P_{\text{H}} = & -\frac{1}{2} m_{\sigma}^2 \sigma^2 - \frac{1}{3} g_2 \sigma^3 - \frac{1}{4} g_3 \sigma^4 + \frac{1}{2} m_{\omega}^2 \omega^2 + \frac{1}{2} m_{\rho}^2 \rho^2 \\ & + \frac{1}{3} \sum_{i=n,p} \frac{1}{\pi^2} \int \frac{k^4}{(k^2 + m_N^{*2})^{1/2}} (f_i^k + \bar{f}_i^k) dk + P_l, \end{aligned} \quad (35)$$

$$\begin{aligned} s_{\text{H}} = & \sum_{i=n,p} \frac{1}{\pi^2} \int dk [-f_i^k \ln f_i^k - (1 - f_i^k) \ln(1 - f_i^k) \\ & - \bar{f}_i^k \ln \bar{f}_i^k - (1 - \bar{f}_i^k) \ln(1 - \bar{f}_i^k)] + s_l, \end{aligned} \quad (36)$$

$$f_{\text{H}} = \varepsilon_{\text{H}} - T s_{\text{H}}. \quad (37)$$

### 3. The Formation of Strangeon Nuggets and the Crossover QCD Phase Transition

In our proposed model, the QCD phase transition is characterized as a continuous crossover phase transition where quarks interact and form strangeon nuggets. During this process, small nuggets quickly decay into nucleons, while large strangeon nuggets can survive even after temperatures decrease below  $T \sim 100$  MeV. The nature of the strongly interacting system, whether it be a nucleon-constituted nucleus or a strangeon-constituted nugget, is determined by the fundamental strong and weak interactions. From an astrophysical standpoint, it is conjectured that bulk strangeon nuggets could be more stable than the nucleus  ${}^{56}\text{Fe}$ .<sup>58</sup> Therefore, strangeon nuggets with a baryon number larger than a critical number  $A_c$  could be long-lived and considered classical particles due to their massive mass. However, those with a baryon number below  $A_c$  will quickly decay into neutrons and establish a nuclear statistical equilibrium with protons since the temperature is still higher than the weak interaction decoupling temperature  $T_{\text{dec}} \sim 1$  MeV. The value of  $A_c$  is determined by the interaction scale and can range from  $A_c \simeq (10^3 \sim 10^9)$ . For example, suppose we only consider the weak decay of the  $s$  quark may cause the instability of the strangeon droplets. In that case, the critical scale is given by the electron Compton wavelength,  $D_c \sim \lambda_c = 2\pi/(m_e c) = 2.4 \times 10^3$  fm, so we have  $A_c \sim \lambda_c^3 \sim 10^9$ . Alternatively, one has  $A_c \simeq 300$  if only the strong interaction is considered.<sup>59</sup> Besides, follow the evaporation rate discussion from Ref. 24 (which gives  $A_c \sim 10^{52}$  for strangelet),

$$\frac{dA}{dt} = \frac{1}{2\pi^2} m_n T^2 e^{-\frac{1}{T}(f_n + f_p)} \sigma_0 A^{\frac{2}{3}}, \quad (38)$$

where  $m_n$  is the nucleon mass,  $T$  is the temperature and  $f_n, f_p$  are absorption efficiencies (for neutrons and protons) correcting the geometric cross-section  $\sigma_0 A^{\frac{2}{3}}$ . The primary difference between strangelets and strangeon nuggets lies in their binding energy  $I$ , and slight variations in  $I$  can significantly impact the stable baryon number  $A$ . Typically, strangeon nuggets have a larger binding energy than strangelets, that a small difference of several times in the binding energy  $I$  can result in an exponential disparity in the critical baryon number  $A_c$ . Based on the discussion above, we use the suggested value of  $A_c \simeq (10^5 \sim 10^9)$ . To describe the co-existence of hadrons and strangeon nuggets after the phase transition, we use a distribution function of  $A$ . The timescale for the QCD phase transition is approximately  $\sim 10^{-6}$  second, which is much longer than the relaxation timescale for the Universe to achieve thermal equilibrium. Therefore, we define a crossover region near the critical temperature  $T_c$  and use a smooth interpolation of the Helmholtz free energy per baryon to describe the continuous phase transition. However, a realistic calculation would need to consider the hybrid existence of the quark phase and HS phase and integrate the transition process with the strangeon nugget distribution evolution.

### 3.1. Formation of the strangeon nuggets

It is more challenging to form a nugget with a larger baryon number  $A$  through collisions. Consequently, nuggets with larger  $A$  tend to have a lower number density. This is analogous to the behavior in atomic nuclei, where the baryon number of a nucleus is proportional to its volume, given by the relationship  $A = (D/D_0)^3$ , where  $D$  represents the diameter of the nuggets. In this study, we adopt an exponential distribution that depends on the size of the nuggets  $D$ ,

$$n(D) = n_0 e^{-D/R_c} = n_0 e^{-\frac{2D}{D_0 A_c^{1/3}}}, \quad (39)$$

where  $R_c = D_c/2$  is the critical radius for the strangeon nuggets that could be stable.  $n_0$  is the normalization factor since the total number density of the hadron should be

$$\int_0^{D_c} n_0 e^{-D/R_c} dD = 2 \left( \frac{mT}{2\pi} \right)^{3/2} \exp[-(m - \mu)/T] s \quad (40)$$

for the nonrelativistic fermion. This distribution is inspired by the size distribution of raindrops, which encompasses various processes involved in the phase transition between gas and liquid phases. These processes include the condensation of water vapor into rain droplets, evaporation of rain droplets, as well as collisions and merging or fragmentation of rain droplets.

The number density of strangeon nuggets is given by

$$n_S = \int_{D_c}^{\infty} n_0 e^{-D/R_c} dD. \quad (41)$$

The nuggets with  $A > A_c$  form the stable strangeon nuggets that are nonrelativistic, so they should follow the classical Maxwell–Boltzmann velocity distribution.

Then similar to the ideal gas, the EOS reads

$$\begin{aligned}
p &= \frac{1}{3} \int_{D_c}^{\infty} dD n_0 e^{-D/R_c} m_S(D) v(D)_{\text{rms}}^2 \\
&= \frac{1}{3} \int_{D_c}^{\infty} dD n_0 e^{-D/R_c} m_S(D) 4\pi \left[ \frac{m_S(D)}{2\pi T} \right]^{3/2} \int_0^{\infty} dv v^2 \exp \left[ \frac{-m_S(D)v^2}{2T} \right] \\
&= n_S T.
\end{aligned} \tag{42}$$

It is expected that the contribution of antiparticles to the thermodynamic quantities would follow similar relationships as those described by Eqs. (34)–(36). Therefore, the thermodynamic quantities of the system, including the pressure  $P$ , the entropy density  $s$ , the energy density  $\varepsilon$  and the Helmholtz free energy  $f$  can be expressed as follows:

$$p_S = n_{S\pm} T, \tag{43}$$

$$s_S = \int dD n_{S\pm}(D) \left\{ \ln \left[ \frac{(2\pi m_S(D) T)^{3/2}}{n_{S\pm}(D)} \right] + \frac{5}{2} \right\}, \tag{44}$$

$$\varepsilon_S = \frac{3}{2} n_{S\pm} T, \tag{45}$$

$$f_S = \varepsilon_{S\pm} - T s_{S\pm}, \tag{46}$$

$n_{S\pm}$  represents the total number density of particles ( $n_{S+}$ ) and antiparticles ( $n_{S-}$ ).  $\varepsilon_S$  denotes the average kinetic energy density, excluding the contribution from rest mass.

Because of the large number of  $A_c$ , the number density of strangeon nugget is very small compared to the number density of ordinary hadrons, even when accounting for particle–antiparticle pairs. It is typically no more than 10 times the net number density. This can be attributed to the energy release (resulting in entropy decrease) during the formation of strangeon nuggets, which in turn transfers energy to hadrons, causing an increase in entropy. The energy of the HS phase is derived from quark energy. Consequently, the energy density and other thermodynamic quantities of the HS phase are largely independent of the fraction of strangeon nuggets present. Consequently, all these thermodynamic quantities associated with strangeon nuggets are considered negligible in comparison to those of hadrons.

Strangeon nuggets must satisfy chemical potential equilibrium,

$$\mu_S = A(\mu_u + \mu_d + \mu_s) = A\mu_\Lambda = A\mu_n. \tag{47}$$

The total entropy density of hadron and strangeon nuggets should have (with constant  $\frac{s}{n_b}$  as discussed before)

$$s_{HS} = s_H + s_S = n_{bHS} \frac{s}{n_b}. \tag{48}$$

Moreover, since  $D = D_0 A^{1/3}$ , the baryon density of strangeon nugget under this distribution is given by

$$\rho_S = \int_{D_c}^{\infty} dD n_0 \left( \frac{D}{D_0} \right)^3 e^{-D/R_c} dD, \tag{49}$$

then we have the mass density of the ordinary baryons (i.e.  $A < A_c$  component):

$$f_{\text{baryon}} = \frac{\int_0^{D_c} D^3 e^{-D/R_c} dD}{\int_0^\infty D^3 e^{-D/R_c} dD} = 0.1429. \quad (50)$$

Hence, the stable strangeon nuggets are estimated to account for approximately  $\sim 85.7\%$  of the total baryon mass density, offering a potential explanation for dark matter without introducing exotic theories. This ratio is used for the strangeon nuggets and nucleons in HS phase.

Nevertheless, it is important to note that this scenario assumes the stable nuggets are entirely unaffected by other cosmological constraints. For instance, if we only consider the geometric cross-section of the strangeon nuggets, denoted as  $\sigma_{\text{abs}} = \pi R^2$ , the absorption rate of neutrons (since protons are repelled by the surface electrostatic potential for large-sized nuggets) is given by  $dn_n/dt = \sigma_n v_n n_S \propto 1/R = 1/A^{1/3}$ . Our previous study<sup>19</sup> demonstrated that when the nuggets have a uniform size and a baryon number  $A > 10^{25}$ , they remain unaffected by the primordial neutron-to-proton ratio. However, relatively small nuggets may form bound states with light nuclei during the nucleosynthesis epoch. Therefore, a detailed BBN network considering strangeon nuggets becomes necessary to establish realistic constraints on the distribution function of the number density of strangeon nuggets. This topic falls outside the scope of this work, which we will explore in future research.

### 3.2. Crossover phase transition

Building upon the concept introduced in Refs. 60–63, we define the crossover region, commonly referred to as the three-window modeling, centered around the chemical freeze-out temperature  $T_c \sim 170$  MeV, with a temperature range of  $T_c - \Gamma < T < T_c + \Gamma$ , where  $\Gamma$  represents the range of temperatures associated with the QCD phase transition. The EOS of both the quark phase and the HS phase are described in Secs. 2.1 and 2.2 for  $T \gg T + \Gamma$  and  $T \ll T - \Gamma$ , respectively. It is worth noting that the crossover region typically refers to a hybrid state of hadrons and quarks; however, in this work, strangeon nuggets are also included in the hybrid phase and final phase. They coexist and exhibit strong interactions within this crossover region.<sup>60–66</sup> The crossover region that we have discussed is primarily governed by the dynamics of strangeon nuggets. During this hybrid phase, quarks collide and become confined in different-sized strangeon nuggets with a baryon number of  $A$ , which equals one-third of the quark number. At the end of the crossover phase transition, all nuggets with  $A < A_c$  are destroyed and subsequently form nucleons, while components with  $A > A_c$  could survive. To obtain a realistic EOS for the crossover phase transition, a thorough understanding of the evaporation and interaction mechanisms of strangeon nuggets is necessary. This includes the study of evaporation productions and decay timescale for various cluster sizes. However, we do not delve into these mechanisms in our work.

We perform a smooth interpolation of the Helmholtz free energy density  $f$  between the quark phase and the HS phase. This interpolation allows for a continuous description of the system's thermodynamic properties throughout the transition region,

$$f_{\text{Cross}}\left(T; \frac{s}{n_b}\right) = f_{\text{Q}}\left(T; \frac{s}{n_b}\right)\chi_+ + f_{\text{HS}}\left(T; \frac{s}{n_b}\right)\chi_-, \quad (51)$$

where  $\chi_+$  and  $\chi_- = 1 - \chi_+$  are the weight functions. The Helmholtz free energy  $f$  should be the function of number density  $n_b$  and temperature  $T$  (or entropy  $S$ ) under  $\beta$  equilibrium. In the case of the evolving Universe, as the temperature  $T$  decreases while maintaining a fixed value of entropy per baryon  $s/n_b$ , the number density  $n_b$  becomes a function of  $T$ . Hence, it is reasonable to assume that the weight functions  $\chi_+$  and  $\chi_-$  also depend on  $T$  in this scenario,

$$\chi_{\pm} = \frac{1}{2} \left[ 1 \pm \tanh\left(\frac{T - T_c}{\Gamma}\right) \right]. \quad (52)$$

Subsequently, the conservation of  $n_b$  is expressed as

$$n_b = \frac{1}{3} (n_u + n_d + n_s)\chi_+ + (n_p + n_n + n_{A_i})\chi_-. \quad (53)$$

The thermal quantities are described by

$$s_{\text{Cross}}\left(T; \frac{s}{n_b}\right) = s_{\text{Q}}\left(T; \frac{s}{n_b}\right)\chi_+ + s_{\text{HS}}\left(T; \frac{s}{n_b}\right)\chi_-, \quad (54)$$

$$\varepsilon_{\text{Cross}}\left(T; \frac{s}{n_b}\right) = \varepsilon_{\text{Q}}\left(T; \frac{s}{n_b}\right)\chi_+ + \varepsilon_{\text{HS}}\left(T; \frac{s}{n_b}\right)\chi_-, \quad (55)$$

$$P_{\text{Cross}}\left(T; \frac{s}{n_b}\right) = P_{\text{Q}}\left(T; \frac{s}{n_b}\right)\chi_+ + P_{\text{HS}}\left(T; \frac{s}{n_b}\right)\chi_-. \quad (56)$$

#### 4. Results

In Fig. 3, we present the behavior of the strangeon nuggets pressure  $P_S$  (panel (a)) and the total number density of strangeon nuggets and anti-strangeon nuggets  $n_S(\pm)$  (panel (b)) as functions of the cosmic temperature  $T$ . The change in  $P_S$  is consistent with the change in  $n_S(\pm)$ . Other thermodynamic quantities such as  $\varepsilon_S$ ,  $f_S$  and  $s_S$  should exhibit similar behavior to  $n_S(\pm)$  since they are all related to the EOS as shown in Eqs. (43)–(46). We consider different values of the critical baryon number  $A_c$ , specifically  $A_c = 10^5, 10^7, 10^9$ , represented by the red, blue and green lines, respectively. The results include both low and high entropy cases, with  $s/n_b = 100$  (dash-dotted lines) and  $s/n_b = 1.13 \times 10^{10}$  (solid lines), respectively. In Fig. 3 (a), the pressure  $P_S$  arises from the motion of both particles and antiparticles, resulting in a higher pressure at higher temperatures due to the coexistence of these particles and antiparticles. As the temperature decreases to around 120 MeV, most antiparticles annihilate with their corresponding particles (Fig. 3(b)), leading to a decrease in pressure (Fig. 3(a)). Figure 3(b) shows that for larger values of  $A_c$ , the

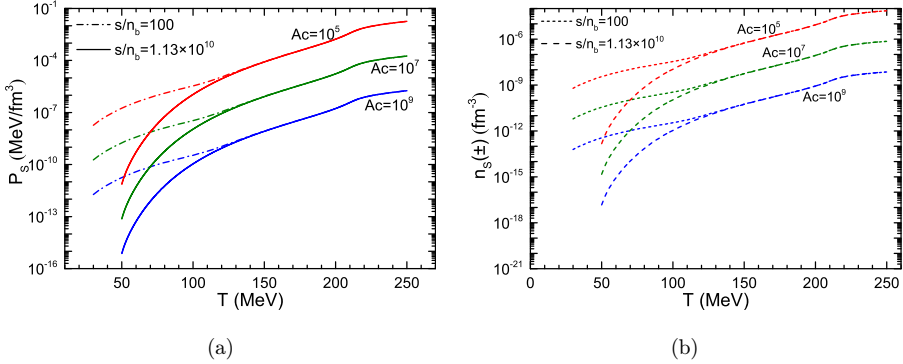


Fig. 3. Panel (a) illustrates the variation of pressure  $P_S$  for strangeon nuggets with respect to temperature  $T$ , while panel (b) depicts the total number density  $n_S(\pm)$ , which includes both particles and antiparticles, as a function of  $T$ .

formed strangeon nuggets contain more baryons, resulting in a smaller number density  $n_S(\pm)$ , and vice versa. Therefore, strangeon nuggets can be treated as clusters of baryonic like matter, and their contribution to the early Universe’s thermodynamics is considered negligible. This is one of the reasons why strangeon nuggets are potential candidates for dark matter.

Figure 4 shows the thermodynamic quantities ( $\varepsilon$ ,  $P$ ,  $s$  and  $f$ ) of both the HS phase and quark phase as a function of temperature  $T$ . Above  $T = 150$  MeV, there is a noticeable rapid increase in  $\varepsilon$ ,  $P$  and  $s$ , which can be attributed to the co-existence of particles and antiparticles in the early Universe at high temperatures. The number density of these particles is approximately proportional to  $T^3$ . Additionally, for high temperatures, the dominant component among elementary particles is free quarks (represented by dash-dotted lines). Their number density is determined by statistical equilibrium, and it decreases significantly at lower temperatures ( $T \sim 150$  MeV), leading to the formation of strangeon nuggets and hadrons (refer to Fig. 5 for more details). Furthermore, at low temperatures, the entropy density of the quark phase (dash-dotted lines in Fig. 4(c)) aligns with that of the HS phase (solid lines in Fig. 4(c)). This can be explained by considering the mass fraction of strangeon nuggets, which accounts for approximately 85% of the total baryon content. Consequently, when all quarks transition into hadrons at low temperatures, the number ratio between HS and quarks becomes approximately  $n_{\text{bHS}} \sim n_{\text{bQ}} \sim 0.85/0.15n_{\text{bH}}$ . On the other hand, the behavior of the Helmholtz free energy  $f$  is opposite that of the other thermodynamic quantities (note that in Fig. 4(d),  $f$  is plotted in absolute value). It is important to note that these thermodynamic quantities should evolve continuously, as outlined in the previous section. Therefore, the phase transition occurs when the interpolation of  $f$ ,  $\varepsilon$  and  $P$  can effectively connect the two phases (refer to Fig. 6 for more details).

Figure 5 illustrates the net baryon number density  $n_b$  (panel (a)) and the total baryon number density  $n_{b\pm}$  (panel (b)) as functions of temperature  $T$ . The net



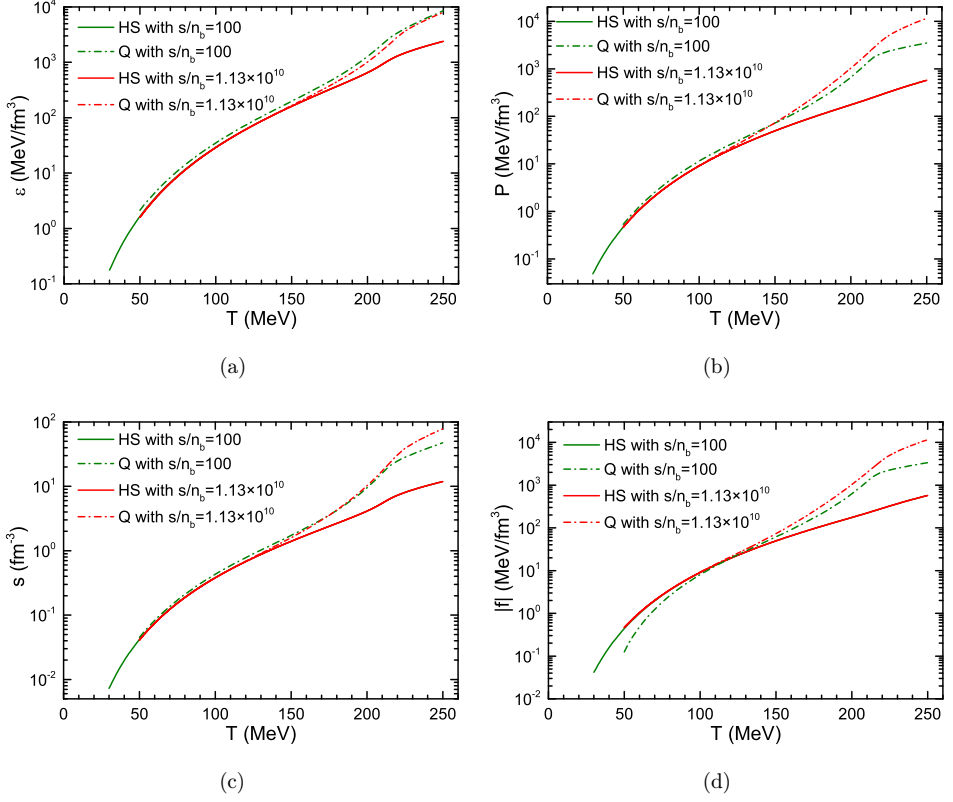


Fig. 4. (Color online) The energy density  $\varepsilon$ , pressure  $P$ , entropy density  $s$  and free energy density  $f$  for HS phase and quark phase as a function of temperature  $T$ . In each panel, the quark phase ( $Q$ ) and the HS phase results are presented in dash-dotted lines and solid lines, respectively. The cases with high entropy are shown in green, while the cases with low entropy are shown in red. Additionally, it should be noted that  $f$  is a negative quantity, and therefore, its absolute value is plotted.

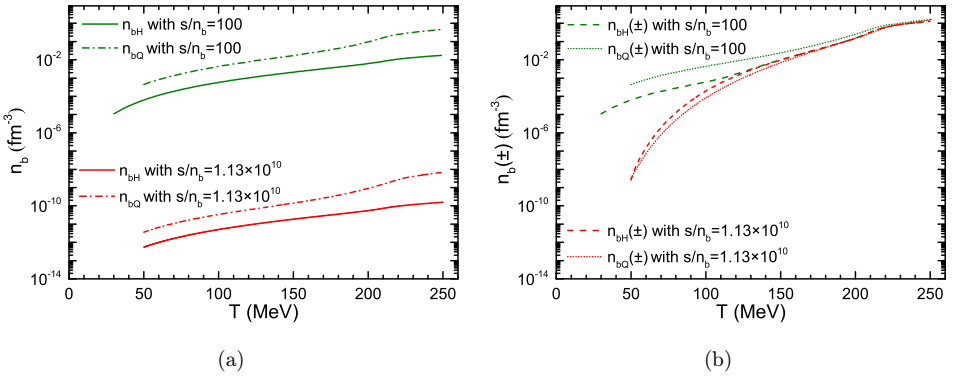


Fig. 5. Panel (a) shows the net baryon number density  $n_b$  for both hadrons and quarks as functions of  $T$ , panel (b) displays the same relation but for the total baryon number density  $n_b(\pm)$ .

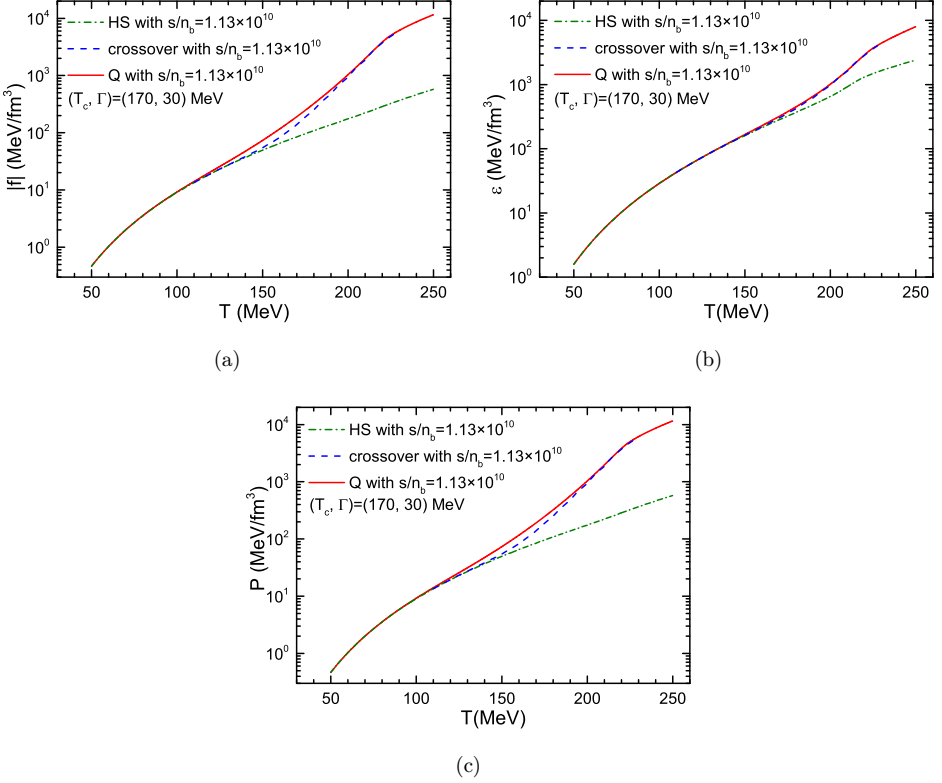


Fig. 6. (Color online) The free energy density  $f$ , energy density  $\varepsilon$  and pressure  $P$  as a function of temperature  $T$  for different phases: the quark phase (solid red line), the crossover region (blue dashed line) and the HS phase (green dash-dotted line). The crossover phase transition takes place at  $(T_c, \Gamma) = (170, 30)$  MeV, i.e. the blue lines represent the interpolation between the red and green lines within this temperature range.

baryon number density  $n_b$  of both phases is shown in dash-dotted lines for the quark phase and solid lines for the HS phase. The total number density  $n_{b\pm}$  is depicted by the dotted lines and dashed lines, respectively. In the Universe, the total number density of baryons  $N_b$  is conserved, so a higher  $s/n_b = S/N_b$  ratio implies a larger entropy  $S$ , which contributes more to the energy at each temperature  $T$ . Conversely, a lower  $s/n_b$  corresponds to less energy, a denser Universe. At high temperatures, particularly above 100 MeV, there is a significant gap between  $n_b$  and  $n_{b\pm}$ . While at low temperatures, most antiparticles annihilate with their counterparts, resulting in  $n_{b\pm}$  being similar to  $n_b$ .

The preceding discussion focuses on the thermodynamic quantities in both the quark and HS phase, which serve as the foundation for the crossover region. As mentioned in Sec. 3.2, all these thermodynamic quantities should undergo continuous changes with cosmic temperature during the crossover phase transition. The relationship for this transition is derived from Eqs. (51) and (54)–(56). In Fig. 6, we

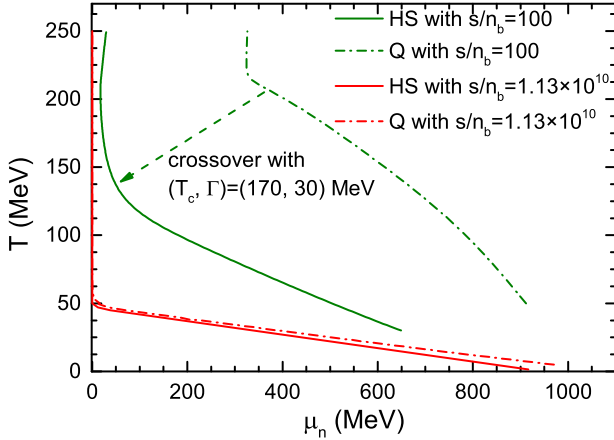


Fig. 7. The QCD phase diagram. Dash-dot and solid lines represent the evolutionary trajectory of the quark phase and HS phase, respectively. The separation between the two phases for the  $s/n_b = 1.13 \times 10^{10}$  is too small to be distinguished in this plot. The dashed arrow is used to indicate the crossover phase transition for the case of  $s/n_b = 100$ .

depict the three-window relation between the thermodynamic quantities ( $f$ ,  $\varepsilon$  and  $P$ ) and the cosmic temperature  $T$ . The three windows correspond to the quark phase (solid lines), the transition window (dashed lines) and the HS phase (dash-dotted lines). The narrow window for the crossover is set at  $(T_c, \Gamma) = (170, 30)$  MeV, and a rapid decrease in energy density  $\varepsilon$  and pressure  $P$  is observed within this region. This trend is indicative of particle–antiparticle pair annihilation.

Furthermore, we present the QCD phase diagram in Fig. 7. The horizontal axis represents the chemical potential of neutrons, for quark phase it is derived from the chemical potential relation  $\mu_n = \mu_d + \mu_u + \mu_s$ . The change of  $\mu_n$  with cosmic temperature  $T$  can be viewed as the trajectory of the QCD transition in the QCD phase diagram. The curves represent the evolutionary trajectories of both the QCD phase (dash-dotted lines) to the HS phase (solid lines). The chemical potential  $\mu_n$  is correlated to the baryon number density  $n_b$ , so a smaller  $s/n_b$  value (larger  $n_b$ ) could shift the trajectory towards the larger  $\mu_n$  side of this figure. We fixed the crossover phase transition at  $(T_c, \Gamma) = (170, 30)$  MeV, and the arrow illustrates this transition for  $s/n_b = 100$ .

## 5. Summary

This study focused on examining the crossover QCD phase transition in the early Universe. At high cosmic temperatures, three flavors of quarks, namely  $u$ ,  $d$  and  $s$  coexist. During the crossover phase transition, these quarks can interact and undergo nucleation to form strangeon nuggets. While smaller nuggets decay rapidly into nucleons, larger nuggets have the potential to remain stable, enabling them to survive the early stages of the Universe. In fact, these stable larger nuggets are


considered as potential candidates for dark matter, which plays a crucial role in the structure and evolution of galaxies and the whole Universe.


In our study, we consider a crossover phase transition occurring at a temperature of approximately  $T \sim 170$  MeV. To describe the thermodynamic quantities in the quark phase at high temperatures, we utilize the PNJL model, while for the hadron phase at low temperatures, we employ the RMF model. We utilize a three-window model, which involves smooth interpolations of the Helmholtz free energy  $f$  between the quark and HS phases. Our analysis shows that when the temperature decreases below 100 MeV, stable strangeon nuggets with different baryon numbers  $A$  can exist. Since it is more difficult to form heavier quark clusters, we employ an exponential distribution function with a critical parameter  $A_c$  to describe the number density of the strangeon nuggets and the nuggets with a baryon number  $A > A_c$  are considered stable. The value of the critical baryon number  $A_c$  is determined by the weak and strong interactions, and in this study, we adopt values of  $10^5, 10^7, 10^9$  based on the discussion before. Due to the large baryon number of the strangeon nuggets, we consider them as noninteracting Boltzmann particles. The results indicate that the contribution of stable strangeon nuggets to the overall thermodynamics of nucleon matter is negligible, which fulfill the features of dark matter. Additionally, the mass density of the strangeon nuggets relative to the baryon matter is approximately  $\sim 0.85/0.15$ , which further supports their potential as candidates for dark matter. The presence of heavy strangeon nuggets has minimal influence on the primordial neutron-to-proton ratio, signifying their potential as candidates for CDM. However, in order to obtain a realistic distribution function of the number density of strangeon nuggets, it is crucial to perform calculations involving a detailed primordial nucleosynthesis network, the abundance prediction of the light elements can serve as the constraint on the mass fraction of the strangeon nuggets. Moreover, the formation of the nuggets during the QCD phase transition could vary the EOS of the early Universe, leave imprints in the induced gravitational wave of the nHz range, which is the detected window of Pulsar Timing Array (PTA). As for experiments of direct detection, an observatory on the quiet moon to monitor its weak quakes might help, since a series of weak moon-quakes could occur when a strangeon nugget penetrates.


## Acknowledgments


We are grateful to Prof. Yuxin Liu and Prof. Motohiko Kusakabe for their helpful suggestion and comments. This work is supported by the National Natural Science Foundation of China under Grant No. 12305148, the National SKA Program of China (No. 2020SKA0120100) and Hebei Natural Science Foundation (No. A2023203055).

## ORCID

Xuhao Wu  <https://orcid.org/0000-0001-5221-2919>

Yudong Luo  <https://orcid.org/0000-0002-8965-1859>

Guo-Yun Shao  <https://orcid.org/0000-0002-1202-1242>

Ren-Xin Xu  <https://orcid.org/0000-0002-9042-3044>

## References

1. A. D. Linde, *Rep. Prog. Phys.* **42** (1979) 389.
2. T. W. B. Kibble, *Phys. Rep.* **67** (1980) 183.
3. A. Mazumdar and G. White, *Rep. Prog. Phys.* **82** (2019) 076901.
4. M. B. Hindmarsh, M. Lüben, J. Lumma and M. Pauly, *SciPost Phys. Lect. Notes* **24** (2021) 1.
5. R. Durrer and A. Neronov, *Astron. Astrophys. Rev.* **21** (2013) 62.
6. V. A. Kuzmin, V. A. Rubakov and M. E. Shaposhnikov, *Phys. Lett. B* **155** (1985) 36.
7. G. R. Farrar and M. E. Shaposhnikov, *Phys. Rev. Lett.* **70** (1993) 2833.
8. A. Kosowsky, M. S. Turner and R. Watkins, *Phys. Rev. Lett.* **69** (1992) 2026.
9. S. Schettler, T. Boeckel and J. Schaffner-Bielich, *Phys. Rev. D* **83** (2011) 064030.
10. T. Boeckel, S. Schettler and J. Schaffner-Bielich, *Prog. Part. Nucl. Phys.* **66** (2011) 266.
11. J. M. Cline, M. Jarvinen and F. Sannino, *Phys. Rev. D* **78** (2008) 075027.
12. S. Weinberg, *Phys. Rev. D* **9** (1974) 3357.
13. P. W. Higgs, *Phys. Rev. Lett.* **13** (1964) 508.
14. E. Witten, *Phys. Rev. D* **30** (1984) 272.
15. A. Bazavov *et al.*, *Phys. Rev. D* **90** (2014) 094503.
16. C. Schmidt and S. Sharma, *J. Phys. G, Nucl. Part. Phys.* **44** (2017) 104002.
17. G. Aarts *et al.*, *Prog. Part. Nucl. Phys.* **133** (2023) 104070.
18. P. J. E. Peebles, *Ann. Phys.* **447** (2022) 169159.
19. X. Y. Lai and R. X. Xu, *J. Cosmol. Astropart. Phys.* **05** (2010) 028.
20. E. W. Kolb and M. S. Turner, *The Early Universe* (Addison-Wesley Publishing, 1990).
21. D. Schwarz, *Ann. Phys.* **12** (2003) 220.
22. Y. Aoki, S. Borsanyi, S. Durr, Z. Fodor, S. D. Katz, S. Krieg and K. K. Szabo, *J. High Energy Phys.* **06** (2009) 088.
23. R. Xu, *AIP Conf. Proc.* **2127** (2019) 020014.
24. C. Alcock and E. Farhi, *Phys. Rev. D* **32** (1985) 1273.
25. J. Madsen, H. Heiselberg and K. Riisager, *Phys. Rev. D* **34** (1986) 2947.
26. X. Y. Lai, C. J. Xia, Y. W. Yu and R. X. Xu, *Res. Astron. Astrophys.* **21** (2021) 250.
27. K. Sumiyoshi and T. Kajino, *Nucl. Phys. B, Proc. Suppl.* **24** (1991) 80.
28. P. Bhattacharjee, J. Alam, B. Sinha and S. Raha, *Phys. Rev. D* **48** (1993) 4630.
29. R. X. Xu, *Astrophys. J.* **596** (2003) L59.
30. X. Lai, C. Xia and R. Xu, *Adv. Phys. X* **8** (2023) 2137433.
31. R. Xu, *Astron. Nachr.* **344** (2023) e230008. arXiv:2212.10887.
32. R. X. Xu, G. J. Qiao and B. Zhang, *Astrophys. J. Lett.* **522** (1999) L109.
33. FAST Collab. (J. Lu *et al.*), *Sci. China Phys. Mech. Astron.* **62** (2019) 959505.
34. X. Y. Lai, C. A. Yun, J. G. Lu, G. L. Lü, Z. J. Wang and R. X. Xu, *Mon. Not. R. Astron. Soc.* **476** (2018) 3303.
35. W. Wang, X. Lai, E. Zhou, J. Lu, X. Zheng and R. Xu, *Mon. Not. R. Astron. Soc.* **500** (2020) 5336.
36. A. Z. Zhou, R. X. Xu, X. J. Wu, N. Wang and X. Y. Hong, *Astropart. Phys.* **22** (2004) 73.
37. C. Peng and R. X. Xu, *Mon. Not. R. Astron. Soc.* **384** (2008) 1034.
38. E. P. Zhou, J. G. Lu, H. Tong and R. X. Xu, *Mon. Not. R. Astron. Soc.* **443** (2014) 2705.
39. Y. Gao, X. Y. Lai, L. Shao and R. X. Xu, *Mon. Not. R. Astron. Soc.* **509** (2021) 2758.

40. H. B. Li, Y. Gao, L. Shao, R. X. Xu and R. Xu, *Mon. Not. R. Astron. Soc.* **516** (2022) 6172.
41. R. Ouyed, D. Leahy, N. Koning and P. Jaikumar, arXiv:2302.06820.
42. B. J. Carr and S. W. Hawking, *Mon. Not. R. Astron. Soc.* **168** (1974) 399.
43. D. K. Nadezhin, I. D. Novikov and A. G. Polnarev, *Astron. Zh.* **55** (1978) 216.
44. G. R. Farrar, *Int. J. Theor. Phys.* **42** (2003) 1211.
45. G. R. Farrar, arXiv:2201.01334.
46. V. V. Flambaum and I. B. Samsonov, *Phys. Rev. D* **105** (2022) 123011.
47. G. Alonso-Álvarez, G. Elor, M. Escudero, B. Fornal, B. Grinstein and J. M. Camalich, *Phys. Rev. D* **105** (2022) 115005.
48. A. R. Zhitnitsky, *J. Cosmol. Astropart. Phys.* **10** (2003) 010.
49. J. N. Guenther, *Eur. Phys. J. A* **57** (2021) 136.
50. A. Bzdak, S. Esumi, V. Koch, J. Liao, M. Stephanov and N. Xu, *Phys. Rep.* **853** (2020) 1.
51. C. S. Fischer, *Prog. Part. Nucl. Phys.* **105** (2019) 1.
52. C. H. Lineweaver and C. Egan, *Phys. Life Rev.* **5** (2008) 225.
53. M. W. Zemansky and R. H. Dittman, *Heat and Thermodynamics*, 1st edn. (McGraw-Hill, New York, NY, USA, 1997).
54. Planck Collab. (N. Aghanim et al.), *Astron. Astrophys.* **641** (2020) A6.
55. P. Rehberg, S. P. Klevansky and J. Hüfner, *Phys. Rev. C* **53** (1996) 410.
56. C. Ratti, M. A. Thaler and W. Weise, *Phys. Rev. D* **73** (2006) 014019.
57. N. K. Glendenning and S. A. Moszkowski, *Phys. Rev. Lett.* **67** (1991) 2414.
58. X. Y. Lai and R. X. Xu, *J. Phys. Conf. Ser.* **861** (2017) 012027.
59. Z. Wang, J. G. Lu and R. X. Xu, *JPS Conf. Proc.* **20** (2018) 011032.
60. K. Masuda, T. Hatsuda and T. Takatsuka, *Prog. Theor. Exp. Phys.* **2013** (2013) 073D01.
61. K. Masuda, T. Hatsuda and T. Takatsuka, *Astrophys. J.* **764** (2013) 12.
62. K. Masuda, T. Hatsuda and T. Takatsuka, *Prog. Theor. Exp. Phys.* **2016** (2016) 021D01.
63. K. Masuda, T. Hatsuda and T. Takatsuka, *Eur. Phys. J. A* **52** (2016) 65.
64. D. L. Whittenbury, H. H. Matevosyan and A. W. Thomas, *Phys. Rev. C* **93** (2016) 035807.
65. C.-M. Li, Y. Yan, J.-J. Geng, Y.-F. Huang and H.-S. Zong, *Phys. Rev. D* **98** (2018) 083013.
66. T. Kojo, P. D. Powell, Y. Song and G. Baym, *Nucl. Phys. A* **956** (2016) 821.